Annals of Nuclear Energy 114 (2018) 122–128

Contents lists available at ScienceDirect

Annals of Nuclear Energy

journal homepage: www.elsevier.com/locate/anucene

Numerical investigation on the bubble separation in a gas-liquid separator applied in TMSR

Yin Junlian, Qian Yalan, Zhang Tingting, Wang Dezhong *

School of Nuclear Science and Engineering, Shanghai Jiao Tong University, China

ARTICLE INFO

Article history:
Received 22 July 2017
Received in revised form 23 November 2017
Accepted 3 December 2017

Keywords:
Bubble
Swirl flow
Gas separation
CFD
TMSR

ABSTRACT

The fission gas removal system plays a critical role in the development of the Thorium Molten Salt reactors. An axial gas-liquid separator is adopted in the gas removal system. To predict the bubble trajectories in swirling flow is essential for designing such gas-liquid separator, since the separation efficiency is closely related to the bubble trajectory. In this paper, we proposed a numerical method to predict the bubble motion. This method is a modified Lagrangian approach in that the velocity of the continuous phase is obtained by approximating the velocity profiles from CFD. Combing the known velocity distribution with explicit mathematical expression and the force model for a single bubble, a mathematical model to calculate the bubble motion is well posed. Calculations with various bubble sizes and Reynolds numbers were carried out. By comparing the simulation results with the experimental data, we concluded that the numerical results agree well with the experimental data. The maximum error of the separation length is less than 10%, which is accurate enough for the determination of the dimension of the separator.

1. Introduction

Molten salt reactors are engaging more and more interests in the Generation Ⅳ reactors. One advantage of the liquid fueled Thorium Molten Salt Reactor (TMSR) is that the fuel can be burned up deeply with the use of fission gas removal system. The bubbling degassing approach proposed by Oak Ridge National Laboratory (ORNL) (Molten-Salt Reactor Program, 1972) shown in Fig. 1 can be adopted to remove fission gases effectively. In this approach, small helium bubbles as shown in Fig. 1(a) are injected into the coolant in the primary loop, in which mass transfer as shown in Fig. 1(b) of the fission gases from the salt coolant to the bubbles will take place. Then the bubbles of helium and fission gas mixture can be removed by an axial type gas-liquid separator (Neesse and Dueck, 2007; Davidson, 1988) shown in Fig. 2.

The gas-liquid separator shown in Fig. 2 consists of a swirl vane, a swirl chamber, and a recovery vane. When the bubbly flow passing through the swirl vane, bubbles will be concentrated and an air core is formed (Yin et al., 2015) due to the centripetal force acting on the bubble surface. In this way, the bubbles are degassed from the liquid phase. For a successful separation, it must be guaranteed that all bubbles with different sizes enter into the air core, that requires the axial distance (defined as Separation length) taken by bubbles moving from the periphery of the swirl chamber to the center is less than the swirl chamber length. Thus, an accurate and fast numerical approach to predict the separation length is preferred for the separator design.

The gas-liquid two-phase flow is very complex in that the bubbly flow and stratified flow coexist with intense gas-liquid interfacial area variation due to bubble coalescence and breakup. To numerically simulate the flow by two-fluid models such as the full Eulerian, Eulerian-Lagrangian models (Brennan, 2006; Sripriya et al., 2007; Najafi et al., 2005) is still challenging and time consuming. In this paper, we are aiming to develop an alternative method to predict the bubble's motion, which can avoid the difficulties induced by the two-phase flow simulation. A closely relevant work dealing with bubble's trajectory in swirl flow was carried out by Magaud (Angilella et al., 2003). In his mathematical modeling and experiments on the behavior of an isolated bubble in swirling flow, the liquid velocity profile was assumed as a solid-body rotation supposed to a uniform axial velocity, based on which the interface forces including the drag force, the lift force, the virtual mass force, and the turbulence dispersion force were implemented on the isolated bubble. Since the axial velocity component used in the Magaud's model is assumed to be constant, one issue to be addressed is to take non-uniform distribution the axial velocity component of the swirl flow into consideration. In addition, the circumferential velocity cannot be approximated by

* Corresponding author.
E-mail addresses: yinjunlian435@gmail.com (J. Yin), dzwang@sjtu.edu.cn (D. Wang).

https://doi.org/10.1016/j.anucene.2017.12.009
0306-4549/

Nomenclature

TMSR	Thorium Molten Salt Reactor
Re	Reynolds number
R	radius of swirl chamber
z^*	z/R, dimensionless characteristic of axial distance
r∗	r/R, dimensionless characteristic of radial distance
V_0^*, V_1^*, V_2^*	dimensionless characteristic tangential velocity
R_1^* & R_2^*	dimensionless characteristic vortex radii
a	radius of bubble
d	bubble diameter
m_d & V_d	the mass and volume of a single bubble
ρ_d	density of air
v_d	velocity of the bubble
F	integral force
F_p	pressure gradient
F_d	drag force
F_g	buoyancy force
F_l	lift force
F_m	added mass
a_d	integral acceleration
C_d	drag coefficient
C_l	lift coefficient
C_m	added-mass coefficient of a particle in an in viscid fluid
SL	separation length
Experiment SL	separation length of experiment result
Simulated SL	separation length of simulation result
Ab	air core boundary

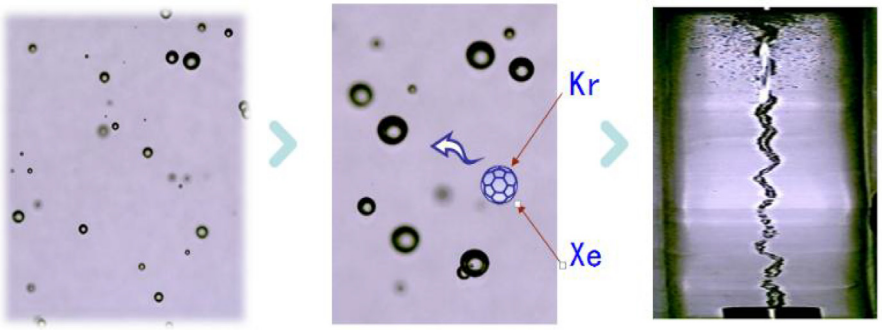

(a) bubble generation (b) mass transfer (c) bubble separation

Fig. 1. Fission gas removal process (a) bubble generation (b) mass transfer (c) bubble separation.

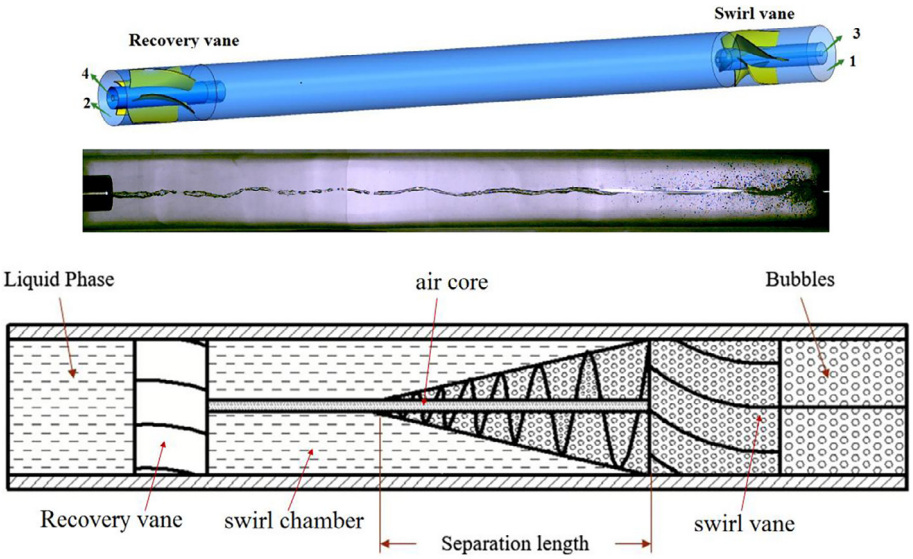

Fig. 2. A typical flow pattern for the gas-liquid separator.

the solid rotation due to that the swirl flow is not generated by rotating the walls of the swirl chamber used by Magaud (Angilella et al., 2003) but by the guiding of the swirl vanes. Thus, by incorporating the exact velocity profiles in the gas-liquid separator, a modified mathematical modeling approach was developed to predict the motion for the isolated bubble, in which the influences induced by bubbles' interaction was neglected because of the low void fraction of the gas phase. Then the model was

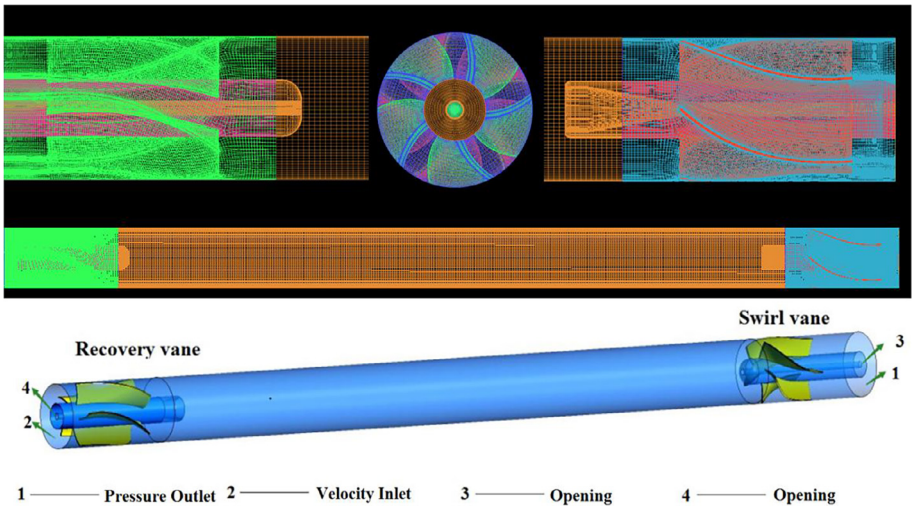

Fig. 3. The grid geometry and boundary conditions in the computation.

validated by comparison with the experimental data obtained in our previous study (Yin, 2017).

2. Mathematical modeling

2.1. Approximation of the velocity field

The three-dimensional (3-D) velocity field was solved by a single-phase simulation of 3-D steady turbulent flow. As for the simulation details such as the geometrical dimensions, the definition of the computational domain, the mesh generation, the turbulence modeling, the boundary conditions and the numerical schemes to discretize the space, readers can refer to a previous two-phase flow simulation by authors (Yin et al., 2015).

CFD models were built to conform to the configuration of the swirl tubes used in the experiments. All geometrical and operational variables, including the shape of swirl vanes and recovery vanes, were faithfully copied in the CFD models of the swirl tube. The three-dimensional models were built in the commercial program UG Graphix, and discretization was performed using ICEM CFD. After generation of the grids they were imported into CFX, which was used for the actual simulations. Fig. 3 shows an overview of the grid geometry.

The grid density was controlled in such a way that the y + of the first grid point of all the walls concerned is less than 1 and the core zone of the swirl chamber is refined to capture the vortex motion more accurately. The total number of cells was 1,00,00,000, including 20,00,000 cells in the swirl vane domain, 20,00,000 cells in the recovery vane domain, and 60,00,000 cells in the swirl chamber domain. As mentioned, pure water was chosen as the working fluid in the simulations. The temperature was taken as 293 K, and the water properties used were: density 997 kg/m3, dynamic viscosity 8.899E-4 Pa-s, and molecular mass 18.02 kg/kmol.

It should be noticed that the selection of turbulence model is very critical for the simulation of the swirling flow. Numerous numerical studies on the swirl flow modeling agreed that the Reynolds stress model (RSM) can be adopted for the turbulence modeling of the steady swirl flow. Thus steady simulations based on the RSM model under several Reynolds numbers (defined by the area averaged velocity in the upstream and the inner diameter of the swirl chamber (R = 25 mm) as the characteristic length) were carried out. Take Re = 56,530 for example, by employing the cylindrical coordinate system shown in Fig. 4, the velocity profiles in terms of the circumferential velocity, the axial velocity, and the radical velocity at different axial locations were extracted in Figs. 5 and 6.

It can be seen from Fig. 4 that the distribution of the circumferential velocity and the axial velocity from $z^* = 0$ to $z^* = 4$ (z^* is dimensionless characteristic as z/R) indicates tends to approach a finalized pattern, which is maintained as z^* increases. The variation of the velocity can be as scribed to the jet-wake flow out of the swirl vane is gradually eliminated due to the strong shearing mixing process. Numberical simulations under several Reynolds numbers validated that the circumferential and axial velocity patterns can be finalized at $z^* = 4$. That explains the foundation based on which the injection position of the single bubble generator is arranged at $z^* = 4$. To approximate the velocity in an analytical

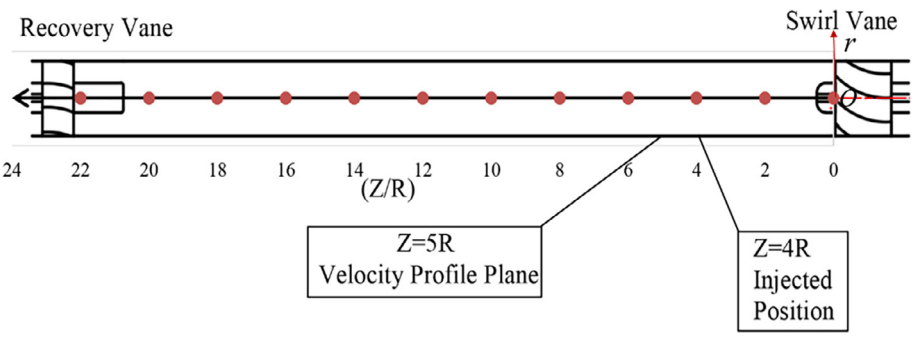

Fig. 4. Coordinate definition for velocity profile analysis.

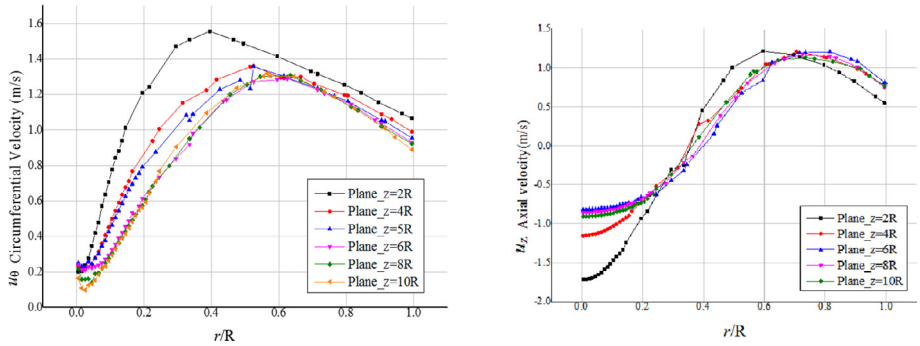

Fig. 5. The velocity profiles at different axial locations.

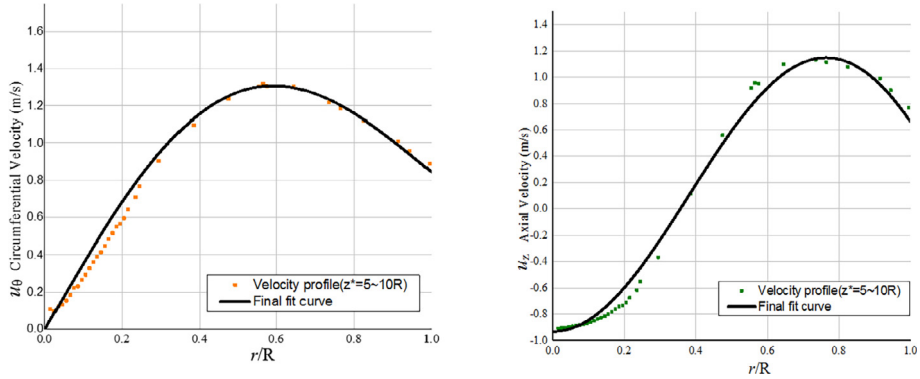

Fig. 6. The velocity profile with fitting curve.

way, various vortex models including the Lamb-Oseen vortex, the Rankie vortex, the Burges vortex, and the Batchlor vortex were adopted for curve fitting work. Finally, based on the study by Liu (Liu and Batchelor Vortex Model, 2015), a simple model based on the Batchlor vortex was proposed to describe the average velocity field ($z^* > 4$) in the swirl chamber. The axial and circumferential velocities can be well approximated by the combination of two coflowing Batchlor vortexes. Eqs. (1) and (2) were used for the curve fitting of the circumferential velocity and the axial velocity, respectively. As the bubble trajectory mainly flows in 5R along the swirl chamber axis in experiment prediction, average of velocity profile for $z^* = 5R$ to $z^* = 10R$ is used as calculation area for the curve fitting. The comparison between the curve approximation and the CFD velocity profile is presented in Fig.5. In addition, we found that the radial velocity can be small enough to be ignored compares to the circumferential and axial velocity. Thus, the flow field of the liquid phase can be represented by Eqs. (1) and (2), which will be incorporated in the following to develop the mathematical model for the motion of a single bubble.

$$\begin{cases} \frac{\bar{u}_\theta(r)}{U_j} = V_0^* r^* + \frac{V_1^* R_1^{*2}}{r^*}\left[1 - exp\left(-\frac{r^{*2}}{R_1^{*2}}\right)\right] + \frac{V_2^* R_2^{*2}}{r^*}\left[1 - exp\left(-\frac{r^{*2}}{R_2^{*2}}\right)\right] \\ \frac{\bar{u}_z(r)}{U_j} = U_0^* + U_1^* \exp\left(-\frac{r^{*2}}{R_1^{*2}}\right) + U_2^* \exp\left(-\frac{r^{*2}}{R_2^{*2}}\right) \end{cases} \quad (1)$$

where the axial and circumferential velocities are normalized by the inlet velocity, Uj; The dimensionless radial position r^* is set as r/R.; V_0^*, V_1^*, V_2^* are dimensionless characteristic tangential velocity; R_1^* and R_2^* are dimensionless characteristic vortex radii; and U_0^*, U_1^*, U_2^* are dimensionless characteristic axial velocities. These eight coefficients are fitted by the nonlinear fitting functions shown in Fig. 6. Reader can refer to Reference Liu and Batchelor Vortex Model (2015)).

2.2. Modeling of forces acting on the bubble

Assuming a single bubble as spherical shape with a radius of a, the integral force acting on a single bubble can be expressed as:

$$F = F_p + F_d + F_g + F_l + F_m = m_d a_d = \rho_d V_d \frac{dv_d}{dt} \quad (2)$$

where F denotes the integral force, F_p denotes the pressure gradient, F_d denotes the drag force, F_g is the buoyancy, F_l is the lift force, F_m is the added mass, m_d and V_d is the mass and volume of a single bubble, a_d is the integral acceleration, ρ_d is the density of air and v_d is the velocity of the bubble. Each kind of force presented in Eq. (2) is calculated by Eq. (3).

$$\begin{cases} F_p = \rho_c V_d \frac{dv_c}{dt} \\ F_d = -\frac{1}{2}\rho_c C_d \pi a^2 (v_d - v_c)|v_d - v_c|, C_d = \frac{24}{\mathrm{Re}}(1 + 0.15\mathrm{Re}^{0.687}) \\ F_g = V_d(\rho_d - \rho_c)g \\ F_l = \rho_c V_d C_l (v_c - v_d) \times \Omega \\ F_m = C_m \rho_c V_d \frac{d(v_c - v_d)}{dt} \end{cases} \quad (3)$$

where C_d is the drag coefficient which depends on the bubble Reynolds number, C_l is the lift coefficient which is assumed to be 1/2 for spherical bubbles, $\Omega = \mathrm{curl}\ V_c$, C_m denotes the added-mass coefficient of a particle in an in viscid fluid. Substituting Eq. (3) into Eq. (2) will yield,

$$\begin{aligned} \rho_d V_d \frac{dv_d}{dt} = {} & \rho_c V_d \frac{dv_c}{dt} - \frac{1}{2}\rho_c C_d \pi a^2 (v_d - v_c)\|v_d - v_c\| \\ & + V_d(\rho_d - \rho_c)g + \rho_c V_d C_l (v_c - v_d) \times \Omega \\ & + C_m \rho_c V_d \frac{d(v_c - v_d)}{dt} \end{aligned} \quad (4)$$

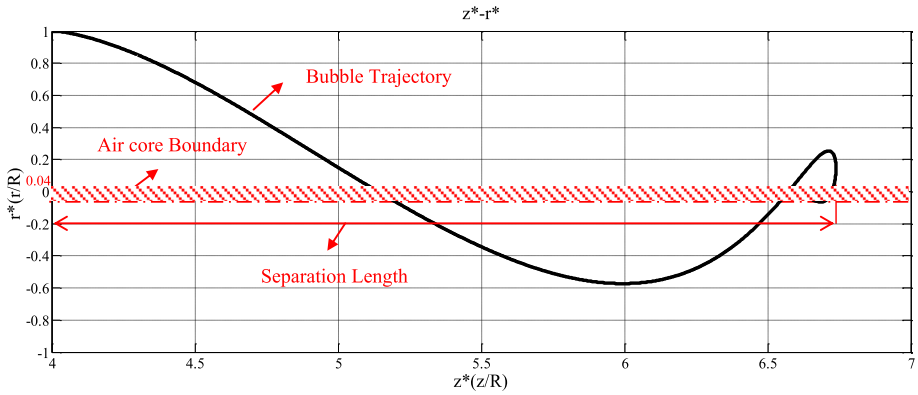

Fig. 7. Constrains and conditions used in the calculation of bubble's separation length.

where V_d indicates the volume of the bubble and ρ_d is the bubble density. To solve Eq. (4) in Matlab, the Runge-Kutta method is used in the cylindrical coordinate system. The initial and boundary conditions were set such that, at $t = 0$, the single bubble was located at the position where the bubble was injected in the measurement ($z = 4R$, $r = R$, $\theta = 0$) with the initial velocity equivalent to that of the liquid phase. The bubble is assumed to be captured by the air core when the radial position of the bubble is less than $r/R = 0.04$ (Based on the fact that air core diameter measured in the experiments about 0.04R. The longest axial distance the bubble takes from the peripheral position into $r/R = 0.04$ is defined as the separation length, which is illustrated in Fig. 7.

3. Results and discussion

To validate the numerical model, boundary conditions were set to cover a wide range of bubble diameters from 0.2 mm to 1.2 mm and of Reynolds numbers from 40,000 to 1,00,000. The comparison between the experimental data and the numerical results was made in twofold: the comparison of bubble trajectories during the separating process and the comparison of the overall separation length. Fig. 8 shows the comparison between the measured and calculated bubble trajectories projected on the y-z plane for two bubble sizes, d = 0.54 mm and 1.033 mm when Re = 70,658. The calculated trajectory denoted by the dash lines agrees well with the measured one denoted by normal lines, which also clearly indicates that the separation length tends to increase as the bubble diameter decreases. As for the separation trajectory itself, a notable phenomenon observed in the experiment that the bubble will move inward more rapidly when approaching the air core were also well predicted for both cases. In addition to validations for the bubble size effects, Fig. 9 shows the comparisons of the bubble trajectories under two Reynolds numbers for the bubble diameter of d = 0.54 mm. Similar agreement between the measured data and the calculated results can be seen and basically the tendency of the separation length variation with the Reynolds number can be reproduced by the model developed. Figs. 8 and 9 provide sufficient confidence to extend this model to predict the effects of the bubble size and the Reynolds number on the separation lengths.

Using the method introduced in Section 2 to determine the separation length, calculations with different bubble sizes ranging from 0.2 mm to 1.1 mm were conducted and the calculated results were compared with the measured data in Fig. 10, from which it can be seen that the separation length was underestimated with a maximal relative error up to 8%. Fig. 11 shows the comparison of the dependence of the separation length on the Reynolds number with two groups of bubble size. Again, the underestimation of the separation length was found for all the Reynolds numbers covered, in which the maximal relative error approaches to 10%. The gap of the numerical error can be attributed to the modeling for the drag force, the lift force, etc. Since all the correlations coefficients presented in Eq. (3) are based on the assumption of spherical bubbles, however, the bubbles dispersed in the swirl flow regime are presented in the form of specially distorted shape. It was observed from the visualization experiment that the bubble is always elongated into oblate ellipsoid or spherical cap. For a given bubble with the same volume, the distorted bubble will experience

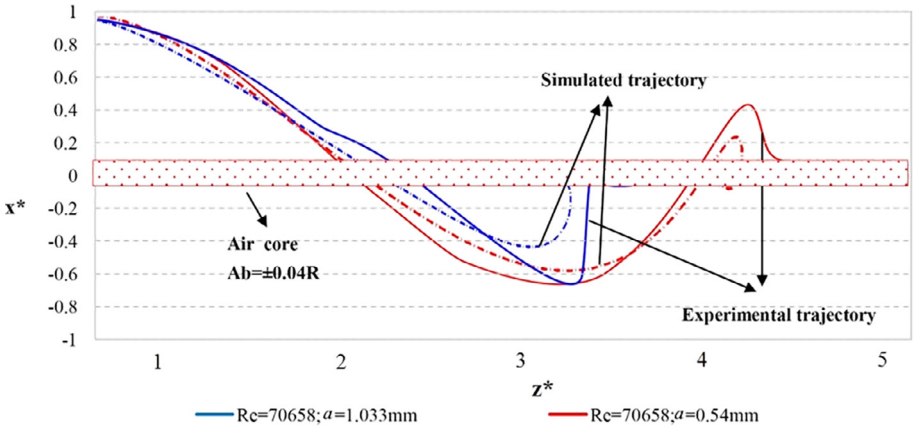

Fig. 8. Comparison of bubble separation trajectories with two bubble sizes under Re = 70,658 (Experimental data cited from Reference Yin et al. (2015)).

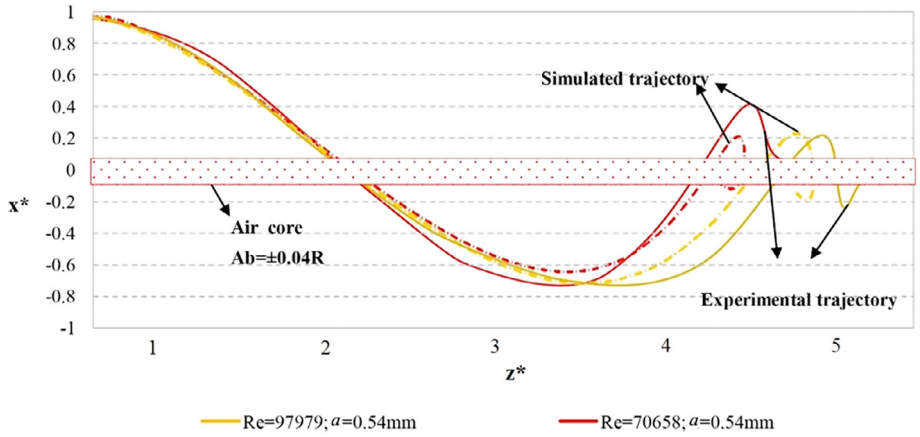

Fig. 9. Comparison of bubble separation trajectories with two Reynolds numbers under bubble size d = 0.54 mm (Experimental data cited from Reference Yin et al. (2015)).

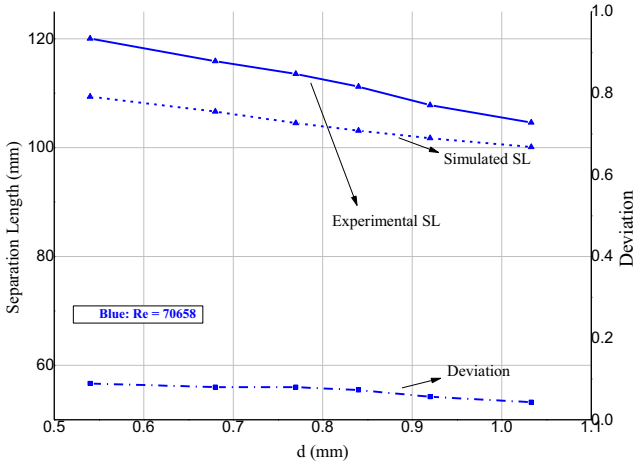

Fig. 10. Comparison of the bubble separation length vs. bubble diameter under Re = 70,658.

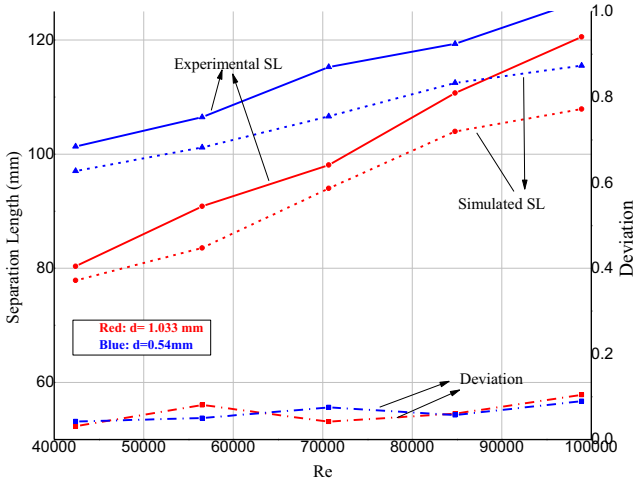

Fig. 11. Comparison of the bubble separation length vs. Reynolds number under bubble size d = 1.033 and 0.54 mm.

smaller pressure gradient force and larger drag force. Thus the predicted separation length is always lower than experimental results. Another error source from the modeling of the interaction between the bubble and the liquid phase is the bubble size variation with the changing pressure field. In that regard, one bubble dynamics equation used to describe the relation between the bubble diameter and the pressure and velocity field should be further incorporated.

4. Conclusion

In this study, we explored a new numerical method to predict the trajectory of a single bubble in a gas-liquid separator. Following the Lagrangian approach, the equation governing the motion of the single bubble was built by relating the forces including the drag force, the lift force, the bouncy force, and the virtual mass force to the averaged velocity field, which can be well approximated by a combination of two Bachelor vortexes. A comparison of the circumferential and axial velocity profiles between the Bachelor vortex model and the CFD results based on the RSM turbulence closure model shows a well agreement. By incorporating the Bachelor vortex model, a very simple second order ordinary equation for the bubble motion was established and can be solved very fast compared with other two phase flow modeling approaches. The mathematical model was validated against with experimental data sets with different bubble sizes and different Reynolds numbers. Comparing the calculated bubble separation trajectory and the overall separation length with the experimental data indicates that the calculated trajectories follows well with the measured, and the maximal error of the overall separation length is less than 10%. These provide some guidelines to improve the accuracy in the further effort for modeling work.

Acknowledgement

This study is supported by National Natural Science Foundation of China (Nos. 51406114 and 11535009).

References

Angilella, J.R., Souhar, M., 2003. Modeling and qualitative experiments on swirling bubbly flows: single bubble with rossby number of order.
Brennan, M., 2006. CFD simulations of hydrocyclones with an air core: Comparison between large eddy simulations and a second moment closure. Chem. Eng. Res. Des. 84 (6), 495–505.
Davidson, M.R., 1988. Numerical calculations of flow in a hydrocyclone operating without an air core. Appl. Math. Model. 12 (2), 119–128.
Liu, Z. et al., 2015. A Batchelor Vortex Model for Mean Velocity of Turbulent Swirling Flow in a Macroscale Multi-Inlet Vortex Reactor. J. Fluids Eng.-Trans. ASME 137. 0412044.
Najafi, A., Saidia, M.H., Sadeghipour, M.S., et al., 2005. Numericalanalysis of turbulent swirling decay pipe flow. Int. Commun. Heat Mass Transfer 32, 627–638.

Neesse, T., Dueck, J., 2007. Air core formation in the hydrocyclone. Miner. Eng. 20 (4), 349–354.
Molten-Salt Reactor Program: Semiannual Progress Report for Period Ending February 29, 1972. Oak Ridge National Laboratory, 1972.
Sripriya, R., Kaulaskar, M.D., Chakraborty, S., et al., 2007. Studies on the performance of a hydrocyclone and modeling for flow characterization in presence and absence of air core. Chem. Eng. Sci. 62 (22), 6391–6402.
Yin, J.L. et al., 2017. Experimental study on the bubble trajectory in an axial gas-liquid separator applied for tritium removal for molten salt reactors. Nucl. Eng. Des. 320, 133–140.
Yin, J., Li, J., Ma, Y., et al., 2015. Study on the air core formation of a gas–liquid separator. J. Fluids Eng. 137 (9), 091301.
Yin, J., Li, J., Ma, Y., et al., 2015. Numerical approach on the performance prediction of a gas–liquid separator for TMSR. J. Nucl. Sci. Technol., 1–8